NANO LETTERS

Letter

pubs.acs.org/NanoLett

Scanning Single Quantum Emitter Fluorescence Lifetime Imaging: Quantitative Analysis of the Local Density of Photonic States

Andreas W. Schell,*[,†] Philip Engel,[†] Julia F. M. Werra,[‡] Christian Wolff,[§] Kurt Busch,[‡,§] and Oliver Benson[†]

[†]Humboldt-Universität zu Berlin, Institut für Physik, AG Nanooptik, D-12489 Berlin, Germany

[‡]Humboldt-Universität zu Berlin, Institut für Physik, AG Theoretische Optik & Photonik, D-12489 Berlin, Germany

[§]Max-Born-Institut, D-12489 Berlin, Germany

S *Supporting Information*

ABSTRACT: Their intrinsic properties render single quantum systems as ideal tools for quantum enhanced sensing and microscopy. As an additional benefit, their size is typically on an atomic scale that enables sensing with very high spatial resolution. Here, we report on utilizing a single nitrogen vacancy center in nanodiamond for performing three-dimensional scanning-probe fluorescence lifetime imaging microscopy. By measuring changes of the single emitter's lifetime, information on the local density of optical states is acquired at the nanoscale. Three-dimensional ab initio discontinuous Galerkin time-domain simulations are used in order to verify the results and to obtain additional insights. This combination of experiment and simulations to gather quantitative information on the local density of optical states is of direct relevance for the understanding of fundamental quantum optical processes as well as for the engineering of novel photonic and plasmonic devices.

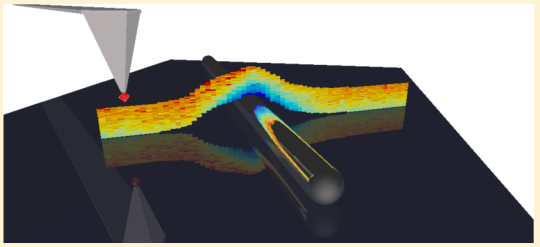

KEYWORDS: *Nitrogen vacancy center, scanning probe microscopy, nanowire, FLIM, discontinuous Galerkin time-domain simulation, plasmonics*

Quantum physics enables measurements with a precision overcoming the classical limit.[1] Therefore, quantum-enhanced sensing has become one of the major fields in quantum technology.[2] Single quantum systems represent ideal sensing probes,[3] not only because of their intrinsic quantum properties, but also because they are typically very small. They can explore local fields of single atoms or a local environment consisting of only a few molecules. Optical quantum probes, such as single quantum emitters, provide the additional advantage of reliable initialization as well as efficient and easy read-out. High sensitivity sensing of electric[4] or magnetic fields[5,6] has been demonstrated. In this paper, we report for the first time on utilizing a single quantum emitter (QE) for performing quantitative three-dimensional scanning-probe fluorescence lifetime imaging microscopy (FLIM) introducing the new technique of QE-FLIM.

We show that in addition to its intrinsically enhanced spatial resolution the ultimate control of a QE-FLIM probe allows for absolute measurements of the electromagnetic environment of arbitrary nanophotonic structures.

First scanning quantum probes that utilize optical emitters have appeared more than 10 years ago[7] in fluorescence microscopy. They detect vacuum fields via modifications of the emitter's spontaneous lifetime which is not an intrinsic property of an emitter, but is rather determined by the local density-of-states (LDOS).

More generally speaking, any light-matter coupling, as described on the fundamental level by a single dipole coupled to modes of the electromagnetic field, can be modified by changing the LDOS. By carefully designing the LDOS, it is possible to significantly enhance the functionality of devices in photonics and plasmonics. Examples are spontaneous emission control for fast optical modulators,[8] for energy-efficient lasing,[9] or for improving light trapping in solar cells.[10] The design of the LDOS is particularly important for engineering fundamental quantum optical few-photon devices, for example, for efficient and fast single photon sources needed in optical quantum information processing systems.[2] Photonic structures such as microcavities,[11] photonic crystals,[12] optical antennas,[13] and photonic metamaterials[14] allow for a design of the LDOS in all three spatial dimensions. Therefore, techniques to obtain precise information about the LDOS on the nanoscale are needed. There exist several approaches to obtain this information, for instance, coating of the structures of interest with fluorescent dyes,[15] mapping with scanning near field microscopes,[16−18] nanopositioning of defect centers[19] or colloidal quantum dots,[20] using optically trapped nanocrystals,[21] or employing a scanning electron microscope.[22] Most of the previous fluorescent probes utilize large ensembles of

Received: February 4, 2014
Revised: March 27, 2014
Published: April 2, 2014

   dx.doi.org/10.1021/nl500460c | *Nano Lett.* 2014, 14, 2623−2627

emitters like molecules in nanobeads[23] to determine the LDOS via the observed lifetime changes.

However, due to averaging over an ensemble with different spatial positions and electromagnetic environments, the excitation decay curve often is multiexponential. This makes it difficult to quantify modifications of the decay dynamics when scanning the probe. Additionally, the ultimate spatial resolution is still given by the diameter of the doped beads and there is no information on the vectorial character of the coupling of the emitters to the nanostructure under investigation.

A fundamental FLIM probe would consist of a single atom. However, single ions in an ultrahigh vacuum environment do not meet the requirement for a robust scanning probe where a pointlike fluorescent dipole is located at a scanning tip, which can be actively stabilized and scanned across an arbitrary substrate. Defect centers in nanodiamonds[24] exhibit ideal properties for this purpose,[19,25,26] since they are optically stable even at room temperature. Here, we use a single-photon emitting nitrogen vacancy (NV) center as a scanning probe for fluorescence lifetime imaging. The single emitter nature of the NV center leads to an increase in obtainable resolution only limited by the size of a single NV center and the mechanical stability of the microscope (for a more detailed discussion see Supporting Information Section IV). There is a clear monoexponential fluorescence decay and the emitter's dipole orientation is a fixed.

The experimental setup is a confocal microscope combined with an atomic force microscope for simultaneous measurements (see Methods and Figure 4 for details). A very important task in quantitative QE-FLIM is the characterization of the probe. It has to be a single emitter with known properties such as orientation, lifetime, and quantum efficiency. All these parameters can be deduced from controlled measurements and comparison to theory (see Methods and Supporting Information). With a fully precharacterized and scanable single quantum emitter, the LDOS can now be mapped on the nanoscale in all three spatial dimensions with high resolution (for a discussion of the term LDOS see Supporting Information Section I). For each position of a scanned area, the detected photons are sorted with respect to the actual height of the oscillating cantilever (see Methods), allowing for continuous feedback while mapping all dimensions of the sample in a single scan. As a result, three-dimensional quantum-emitter fluorescence lifetime microscopy (QE-FLIM) is established.

A first example is shown in Figure 1, where silver nanowires, the drosophila of plasmonics, are raster-scanned by QE-FLIM. Figure 1a,d are AFM topography scans showing a wire and a wire network, respectively. In Figure 1b,e and c,f, lifetimes images are shown for the emitter being in the highest quarter of its tapping mode height oscillation and in the lowest, respectively. The emitter's lifetime decreases close to the surface due to the higher index of refraction and therefore higher LDOS. Close to the nanowire the additional plasmonic modes account for an even more reduced lifetime. In Figure 1d–f, a network of crossed wires is scanned with the QE-FLIM. When scanning along the nearly horizontal wire, the expected decrease of the emitter's lifetime is observed, but also an increase in lifetime is found in a scan parallel to it. This feature is often regarded as a topography artifact in scanning near-field microscopy. Here, we can not only correct it using the recorded full three-dimensional information, but we can also extract

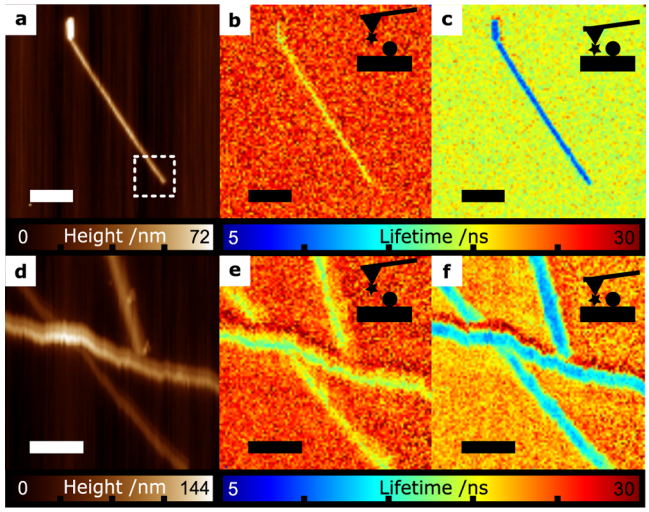

Figure 1. Silver nanowires imaged by QE-FLIM. (a) Atomic force microscope image of a silver nanowire of diameter 50 nm acquired in tapping mode. The dashed rectangle indicates the region, which is investigated in more detail in Figure 2. (b,c) Simultaneously recorded lifetime images for the AFM tip being in the highest quarter of its tapping mode height oscillation and in the lowest, respectively. Scalebars in (a–c) are 1 μm. (d–f) Data for a network of single nanowires. At the nearly horizontal wire in addition to the expected decrease of the lifetime an increase is found. This is a feature stemming from topography and the nanodiamond's position on the tip, which gives information on the NV centers position at the tip. Scalebars are 500 nm. Cantilever oscillation amplitudes are 37 nm for panels b,c and 74 nm in panels e,f, and data acquisition times per pixel are 25 ms for panels b,c and 50 ms in panels e,f.

valuable information on the NV center's position at the AFM tip.

Another striking feature that shows up when looking at silver nanowires, are oscillations of the plasmonic channels of the LDOS along the direction of the wire. They arise due to interference of surface-plasmon polaritions (SPPs) reflected at the wire's ends and the ones directly launched into the wire. When the SPPs are excited by a single emitter as in our case (see Figure 5b) the phenomenon can also be discussed in terms of wave-particle duality.[27] Figure 2 shows a detailed scan of a nanowire's end. Interestingly, the decay of these oscillations away from the wire's ends is much faster than it would be expected by effects of Ohmic plasmon damping and dephasing from the NV center's broad spectrum alone.[28] In order to explain the fast decay it is necessary to take into account higher-order plamonic modes on the silver wire. As confirmed via ab initio three-dimensional discontinuous Galerkin time-domain (DGTD) numerical simulations (see Figure 2h), this multimode nature gives rise to additional dephasing. The observation of this previously disregarded effect demonstrates the power of QE-FLIM, it offers the possibility to study the behavior of the LDOS at the nanoscale in such a controlled way, so that not only qualitative, but also quantitative comparisons with theory are possible. The modulation observed is in phase with the modulation of the lifetime, meaning that more photons are collected when the lifetimes are longer. This behavior is because the additional decay channels, which shorten the lifetime, are of plasmonic nature and bound to the wire. The majority of the plasmons gets either absorbed or leaves the confocal volume of the microscope before getting

dx.doi.org/10.1021/nl500460c | Nano Lett. 2014, 14, 2623–2627

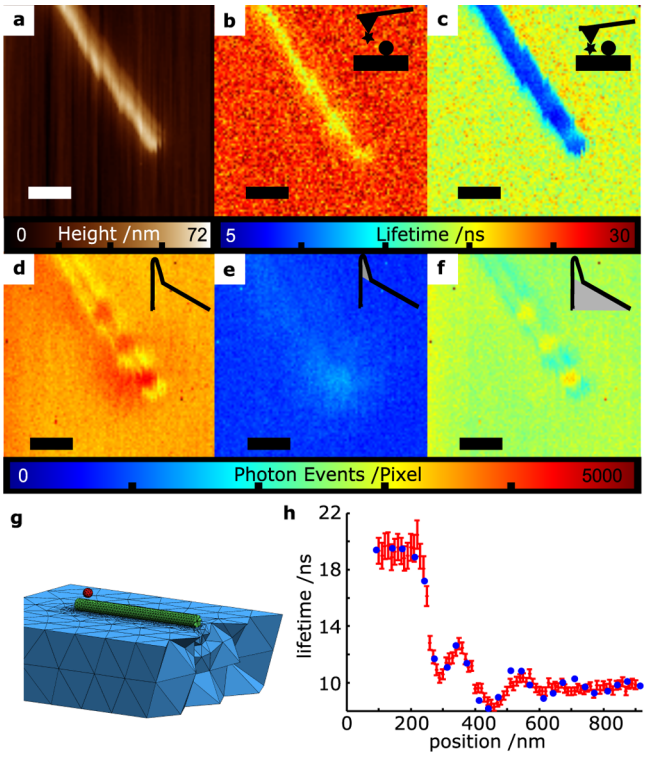

Figure 2. Oscillations of the LDOS at the wire's end. (a) Zoom to the end of a silver wire, as indicated in Figure 1a. (b,c) Lifetime in the upper and lower quarter of the cantilevers oscillation, respectively. (d) Intensity measured while scanning. (e,f) Intensity in the lower quarter of the background photons and the photons stemming from the diamond, respectively. An oscillation of the photonic intensity due to plasmonic modes back reflected at the wire's end is visible. Scalebars are 200 nm and data acquisition time per pixel is 25 ms. (g) Mesh used in the three-dimensional DGTD simulations. The emitter (red) interacts with a silver nanowire (green) lying on a glass substrate (blue). (h) Lifetime dependence of the NV center when scanned along the wire. Big blue dots are results from simulations (for parameters see Methods). An excellent quantitative agreement from ab initio simulations and experimental data is found.

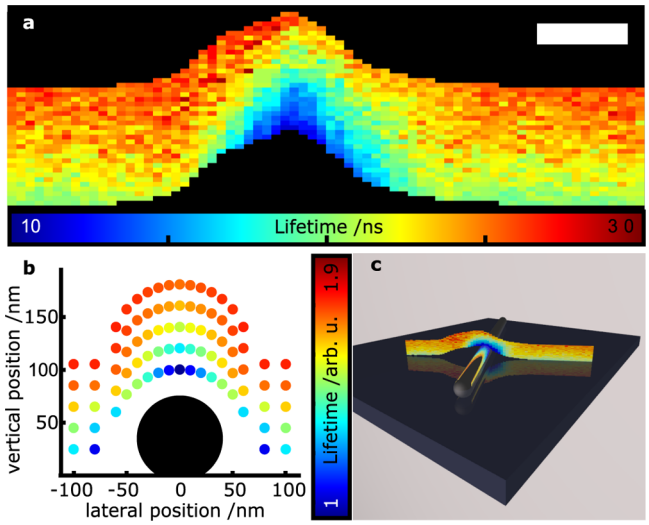

Figure 3. Two-dimensional stripe scan across a silver nanowire. (a) Color-coded lifetime data as a function of height and position perpendicular to a silver nanowire. The absolute height is corrected according to the topography data acquired simultaneously with the AFM. In this way, topography artifacts are corrected as well. Height and position axis are scaled equally and the scalebar is 100 nm. Data acquisition time is 200 ms per pixel. (b) Numerical simulation corresponding to the data in (a). As in (a) the same probe as in Figure 2 is used, the probe parameters used for the simulations correspond. (c) Artists view clarifying the geometry of silver wire and data in panels a,b.

scattered out, an effect often misunderstood as fluorescence quenching.

An additional unique feature of 3D QE-FLIM is the possibility to derive topography-corrected lifetime images. Whereas Figure 1 displays lateral scans for two different relative positions of the scanning cantilever, Figure 3 shows a scan crossing a silver nanowire in a plane perpendicular to the sample surface. The amplitude of the cantilever's oscillation of 128 nm is divided in 25 height bins. At the same time, for each pixel the absolute height of the sample is acquired with the AFM. Therefore, Figure 3a represents a lifetime image with completely known spatial coordinates avoiding artifacts which often appear in scanning probe images. The observed rate enhancement by a factor of 2.6 is of the order that is expected from previous experiments dealing with the coupling of nanodiamonds to silver nanowires.[27,29]

In conclusion, we have introduced QE-FLIM as an ultimate limit of optical scanning probe microscopy. We showed that a stable and fully characterizable pointlike probe is mandatory to go hand-in-hand with full ab initio three-dimensional numerical simulation. By collecting the photons from a single emitter glued to an AFM tip and tagging with the cantilever position, lifetime data in all three dimensions can be acquired in a single scan without topography artifacts. The obtained three-dimensional data sets give detailed insight into the electromagnetic environment at the nanoscale with subdiffraction-limit resolution. Beyond mapping of the local density-of-states the vectorial role of emitter-field coupling is revealed as a crucial information to characterize arbitrary nanophotonic and nanoplasmonic structures.

Methods. *Confocal Microscope.* The optical microscope in this experiment is a home-built sample-scanning inverted confocal microscope (see Figure 4a). An objective with a numerical aperture of 1.35 (UPlanSApo60XO, Olympus) is used to excite the NV center and to collect the single photons. Excitation is done with a picosecond laser at a wavelength of 531 nm with a variable repetition rate (LDH-P-FA-530, Picoquant). A repetition rate of 10 MHz is used when scanning with the QE-FLIM microscope, while a rate of 80 MHz is used for the autocorrelation measurements. Autocorrelation measurements are performed with a Hanbury Brown and Twiss setup sketched in Figure 4d. After spectral filtering avalanche photodiodes (SPCM-AQR-14, PerkinElmer) are used to detect the single photons.

Atomic Force Microscope. A tip scanning atomic force microscope (NanoWizard, JPK Instruments) is mounted on the confocal microscope (see Figure 4a). The nanodiamonds (MSY 0−0.05 GAF, Microdiamant AG) are spin-coated on a cleaned coverslip, precharacterized using the confocal microscope and subsequently attached to the AFM cantilever. A technique similar to the one described by Schell et al.[30] is used to craft the diamonds to the tip. To make the nanodiamonds stick, the cantilevers are dipped in a drop of poly-L-lysine solution.[25] The typical size of the nanodiamonds glued to the tip is about 30 nm. Cantilevers are silicon tapping mode cantilevers (NSG03, NT-MDT), which proved to contribute only very little to

dx.doi.org/10.1021/nl500460c | Nano Lett. 2014, 14, 2623−2627

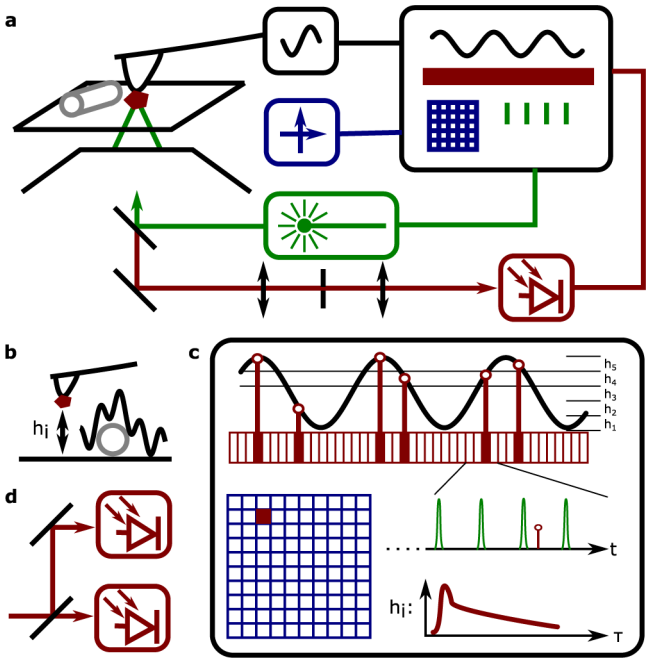

Figure 4. Measurement apparatus and scheme of QE-FLIM. (a) A nanodiamond containing a single NV center is glued to the tip of an AFM cantilever. The AFM is operated in tapping mode and the cantilever is positioned in the focal volume of a scanning confocal microscope equipped with a pulsed laser and an avalanche photodiode. Cantilever oscillation, coordinates, laser timing, and photon time tags are recorded simultaneously. (b) Being operated in tapping mode at different times the AFM tip is at different heights h_i. (c) For each pixel of the scanned sample area, the photon detection events are sorted according to the current height h_i of the AFM tip. In this way, the probe in a single scan reaches different heights with the maximum height being the oscillation's amplitude. The lifetime is determined for different height bins h_i by histogramming the arrival times with respect to the laser pulse and by making a fit to the tail of the exponential decay. This makes it possible to gather real 3D lifetime data while always maintaining feedback from the tapping mode AFM. (d) Scheme of a Hanbury Brown and Twiss interferometer as it is used to prove the single emitter character of the probe.

background fluorescence. While acquiring image data, the nanodiamond probe is positioned in the confocal volume of the microscope and the sample is scanned with a sample scanner.

Electronic Setup and Data Processing. Photon detection event time tags are recorded using a PicoHarp 300 (Picoquant) data acquisition electronic. Markers for spatial coordinates are also fed to the PicoHarp 300 and are collected within the time tag stream. To extract the 3D lifetime information, in addition to the current scanning position, the cantilever's oscillation is also fed to the correlation electronics. With that information, the photon detection events at each pixel of the scanned sample area can be attributed to different height bins. Data in every pixel is histogrammed with respect to the cantilever height and fitted with a monoexponential decay to calculate the lifetime (see Figure 4c). Events in the first 5 ns are not used in order to avoid artifacts from fast decaying background contributions. The line scan in Figure 3 was averaged over 50 AFM scans to compensate for drift.

Probe Characterization. The excited state lifetime of the probe can be extracted from the measurements depicted in Figure 5a. Monoexponential decay curve of the NV center's excited state for different situations are shown: black for the nanodiamond on a coverslip (43.5 ± 1.4 ns), blue for the nanodiamond glued to the tip far from the surface (19.8 ± 0.2 ns), and red with the tip close to a silver nanowire (9.2 ± 0.1 ns). After the nanodiamond is glued to the tip, the lifetime only varies when the environment, and therefore the LDOS, changes, for example, when approaching a silver nanowire (red curve in Figure 5a). To prove the single emitter character

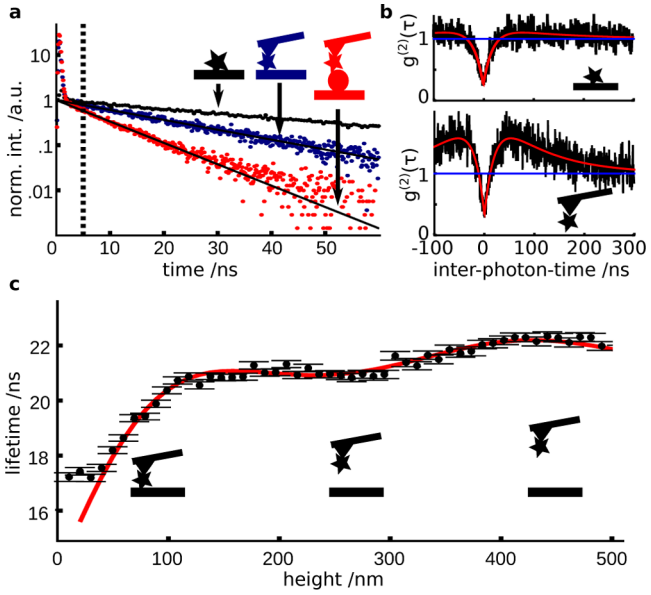

Figure 5. Probe characterization. (a) Lifetime curve of the NV center used in the scans shown in Figures 1−3. The black curve is for the nanodiamond prior to glueing it to the cantilever. A fit yields a lifetime of 43.5 ± 1.4 ns. The blue and red curve are for the diamond on the tip at the glass interface and at a silver nanowire, respectively. Corresponding lifetimes are 19.8 ± 0.2 ns and 9.2 ± 0.1 ns. Only photons after the dotted line are used for lifetime fits. (b) Autocorrelation function $g^{(2)}(\tau)$ of the NV center in a nanodiamond used in the scans lying on a glass coverslip (upper panel) and glued to the AFM tip (lower panel). The red line is a fit to the data according to Jelezko et al.[24] It yields $g^{(2)}(0) = 0.25$ and $g^{(2)}(0) = 0.31$, respectively. A change in the bunching behavior indicates a change in the NV center's environment. Count rates are 120 000/s and 110 000/s, respectively. (c) Lifetime versus height of a nanodiamond probe over a glass surface. The red curves is following an analytical theory for a dipole over a dielectric interface (see also Supporting Information Section III). No background correction was applied to any of the data.

of the probe, measurements of the autocorrelation function $g^{(2)}(\tau)$ are performed using a Hanbury Brown and Twiss setup before and after the nanodiamonds are attached to the tip (see Figure 5b). A value of $g^{(2)}(0) < 0.5$ indicates that the main photon contribution stems from a single emitter. Figure 5c shows detailed data of nanodiamond probes approaching a glass surface. When the emitter approaches the surface, an oscillatory behavior is visible. A careful numerical and analytical analysis examining explicitely the influence of the silicon AFM tip reveals that the approach curves can also be derived in good approximation by an analytical theory. For these theoretical curves, the QE-FLIM probe can be fully characterized, that is, the NV center's orientation, its position within the nanodiamond, as well as the quantum efficiency of its optical transition can be derived (see Supporting Information Section III).

dx.doi.org/10.1021/nl500460c | *Nano Lett.* 2014, 14, 2623−2627

Numerical Simulations. All numerical simulations presented in the manuscript are obtained using the discontinuous Galerkin time-domain method (DGTD).[31,32] A tetrahedral mesh consisting of fourth-order basis functions is used. All material parameters were obtained from measured data and described by the refractive index in the case of dispersionless materials (substrate), and the Drude-Lorentz model for the permittivity of silver, respectively (see Supporting Information Section II). The NV center in the nanodiamond described by two incoherently coupled classical dipoles is computed by determining the complete dyadic Green's tensor and adding the decay rates of two dipoles perpendicular to each other. The spectrum of those dipoles is chosen to resemble a Gaussian spectrum matching the natural spectrum of an NV center (λ = 700 nm, σ = 50 nm). See Supporting Information Section II for further detail on geometry of the setup and Section III for a detailed discussion on the cantilever tip's influence on the results.

Fits of the numerical and analytical data in Figures 2h and 3c, respectively, are done via a least-squares-root fit by applying the Levenberg−Marquardt method. The orientation of the two dipoles of the NV center is described with $d_1 = \sin(\theta)\cos(\varphi)\hat{x} + \sin(\theta)\sin(\varphi)\hat{y} + \cos(\theta)z$ and $d_2 = [\cos(\alpha) \cdot \cos(\theta)\cos(\varphi) - \sin(\alpha) \cdot \sin(\varphi)]\hat{x} + [\cos(\alpha) \cdot \cos(\theta)\sin(\varphi) + \sin(\alpha) \cdot \cos(\varphi)]\hat{y} - \cos(\alpha) \cdot \sin(\theta)\hat{z}$ (θ, φ, azimuthal and polar angle; $\hat{x}$, $\hat{y}$, $\hat{z}$, Cartesian unit vectors). Additionally, the quantum yield QY is adjusted. This leads to QY = 0.5869, $\theta = 0.5174\pi$, $\varphi = 1.2509\pi$ and $\alpha = 1.19\pi$ in Figures 2h and 3b and QY = 0.703 and $\cos(\theta)^2 + \cos(\alpha)^2\sin(\theta)^2 = 0.40$ in Figure 5c.

■ ASSOCIATED CONTENT

Supporting Information

Discussion of the LDOS for a NV center. Numerical simulation and characterization of the probe. Discussion of the spatial resolution of QE-FLIM. This material is available free of charge via the Internet at http://pubs.acs.org.

■ AUTHOR INFORMATION

Corresponding Author

*E-mail: andreas.schell@physik.hu-berlin.de.

Notes

The authors declare no competing financial interest.

■ ACKNOWLEDGMENTS

Support from DFG (FOR1493) is acknowledged. J.F.M.W., K.B., and O.B. acknowledge the support by the Deutsche Forschungsgemeinschaft (DFG) through the Collaborative Research Centre 951 'Hybrid Inorganic/Organic Systems for Optoelectronics (HIOS)' within projects B1 and B10.

■ REFERENCES

(1) Jaekel, M. T.; Reynaud, S. *EPL* **1990**, *13*, 301.
(2) O'Brien, J. L.; Furusawa, A.; Vuckovic, J. *Nat. Photonics* **2009**, *3*, 687−695.
(3) Sekatskii, S.; Letokhov, V. *J. Exp. Theor. Phys. Lett.* **1996**, *63*, 319−323.
(4) Dolde, F.; Fedder, H.; Doherty, M. W.; Nobauer, T.; Rempp, F.; Balasubramanian, G.; Wolf, T.; Reinhard, F.; Hollenberg, L. C. L.; Jelezko, F.; Wrachtrup, J. *Nat. Phys.* **2011**, *7*, 459−463.
(5) Balasubramanian, G.; Chan, I. Y.; Kolesov, R.; Al-Hmoud, M.; Tisler, J.; Shin, C.; Kim, C.; Wojcik, A.; Hemmer, P. R.; Krueger, A.; Hanke, T.; Leitenstorfer, A.; Bratschitsch, R.; Jelezko, F.; Wrachtrup, J. *Nature* **2008**, *455*, 648−651.
(6) Tetienne, J.-P.; Rondin, L.; Spinicelli, P.; Chipaux, M.; Debuisschert, T.; Roch, J.-F.; Jacques, V. *New J. Phys.* **2012**, *14*, 103033.
(7) Michaelis, J.; Hettich, C.; Mlynek, J.; Sandoghdar, V. *Nature* **2000**, *405*, 325−328.
(8) Englund, D.; Faraon, A.; Majumdar, A.; Stoltz, N.; Petroff, P.; Vuckovic, J. *Opt. Express* **2009**, *17*, 18651−18658.
(9) Fujita, M.; Takahashi, S.; Tanaka, Y.; Asano, T.; Noda, S. *Science* **2005**, *308*, 1296−1298.
(10) Callahan, D. M.; Munday, J. N.; Atwater, H. A. *Nano Lett.* **2012**, *12*, 214−218.
(11) Vahala, K. J. *Nature* **2003**, *424*, 839−846.
(12) Hoeppe, U.; Wolff, C.; Küchenmeister, J.; Niegemann, J.; Drescher, M.; Benner, H.; Busch, K. *Phys. Rev. Lett.* **2012**, *108*, 043603.
(13) Novotny, L.; van Hulst, N. *Nat. Photonics* **2011**, *5*, 83−90.
(14) Cortes, C. L.; Newman, W.; Molesky, S.; Jacob, Z. *J. Opt.* **2012**, *14*, 063001.
(15) Hoogenboom, J. P.; Sanchez-Mosteiro, G.; Colas des Francs, G.; Heinis, D.; Legay, G.; Dereux, A.; van Hulst, N. F. *Nano Lett.* **2009**, *9*, 1189−1195.
(16) Imura, K.; Nagahara, T.; Okamoto, H. *J. Chem. Phys.* **2005**, *122*, 154701.
(17) De Wilde, Y.; Formanek, F.; Carminati, R.; Gralak, B.; Lemoine, P.-A.; Joulain, K.; Mulet, J.-P.; Chen, Y.; Greffet, J.-J. *Nature* **2006**, *444*, 740−743.
(18) Beams, R.; Smith, D.; Johnson, T. W.; Oh, S.-H.; Novotny, L.; Vamivakas, A. N. *Nano Lett.* **2013**, *13*, 3807−3811.
(19) Schell, A. W.; Kewes, G.; Hanke, T.; Leitenstorfer, A.; Bratschitsch, R.; Benson, O.; Aichele, T. *Opt. Express* **2011**, *19*, 7914−7920.
(20) Ropp, C.; Cummins, Z.; Nah, S.; Fourkas, J. T.; Shapiro, B.; Waks, E. *Nat. Commun.* **2013**, *4*, 1447.
(21) Geiselmann, M.; Juan, M. L.; Renger, J.; Say, J. M.; Brown, L. J.; de Abajo, F. J. G.; Koppens, F.; Quidant, R. *Nat. Nanotechnol.*. **2013**, *8*, 175−179.
(22) Sapienza, R.; Coenen, T.; Renger, J.; Kuttge, M.; van Hulst, N. F.; Polman, A. *Nat. Mater.* **2012**, *11*, 781−787.
(23) Frimmer, M.; Chen, Y.; Koenderink, A. F. *Phys. Rev. Lett.* **2011**, *107*, 123602.
(24) Jelezko, F.; Wrachtrup, J. *Phys. Status Solidi A* **2006**, *203*, 3207−3225.
(25) Cuche, A.; Drezet, A.; Sonnefraud, Y.; Faklaris, O.; Treussart, F.; Roch, J.-F.; Huant, S. *Opt. Express* **2009**, *17*, 19969−19980.
(26) Maletinsky, P.; Hong, S.; Grinolds, M. S.; Hausmann, B.; Lukin, M. D.; Walsworth, R. L.; Loncar, M.; Yacoby, A. *Nat. Nanotechnol.*. **2012**, *7*, 320−324.
(27) Kolesov, R.; Grotz, B.; Balasubramanian, G.; Stohr, R. J.; Nicolet, A. A. L.; Hemmer, P. R.; Jelezko, F.; Wrachtrup, J. *Nat. Phys.* **2009**, *5*, 470−474.
(28) Ditlbacher, H.; Hohenau, A.; Wagner, D.; Kreibig, U.; Rogers, M.; Hofer, F.; Aussenegg, F. R.; Krenn, J. R. *Phys. Rev. Lett.* **2005**, *95*, 257403.
(29) Huck, A.; Kumar, S.; Shakoor, A.; Andersen, U. L. *Phys. Rev. Lett.* **2011**, *106*, 096801.
(30) Schell, A. W.; Kewes, G.; Schröder, T.; Wolters, J.; Aichele, T.; Benson, O. *Rev. Sci. Instr.* **2011**, *82*, 073709.
(31) Niegemann, J.; König, M.; Stannigel, K.; Busch, K. *Photonics Nanostruct. Fundam. Appl.* **2009**, *7*, 2−11.
(32) Busch, K.; König, M.; Niegemann, J. *Laser Photonics Rev.* **2011**, *5*, 773−809.